PCCP

Accepted Manuscript

ROYAL SOCIETY OF CHEMISTRY

www.rsc.org/pccp

Cite this: DOI: 10.1039/c0xx00000x

www.rsc.org/xxxxxx

ARTICLE TYPE

Computational Raman spectroscopy of organometallic reaction products in lithium and sodium-based battery systems

Roel S. Sánchez-Carrera, and Boris Kozinsky*

Received (in XXX, XXX) Xth XXXXXXXXX 20XX, Accepted Xth XXXXXXXXX 20XX

DOI: 10.1039/b000000x

A common approach to understanding surface reaction mechanisms in rechargeable lithium-based battery systems involves spectroscopic characterization of the product mixtures and matching of spectroscopic features to spectra of pure candidate reference compounds. This strategy, however, requires separate chemical synthesis and accurate characterization of potential reference compounds. It also assumes that atomic structures are the same in the actual product mixture as in the reference samples. We propose an alternative approach that uses first-principles computations of spectra of the possible reaction products and by-products present in advanced battery systems. We construct a library of computed Raman spectra for possible products, achieving excellent agreement with reference experimental data, targeting solid-electrolyte interphase in Li-ion cells and discharge products of Li-air cells. However, the solid-state crystalline structure of Li(Na) metal-organic compounds is often not known, making the spectra computations difficult. We develop and apply a novel technique of simplifying spectra calculations by using dimer-like representations of the solid state structures. On the basis of a systematic investigation, we demonstrate that molecular dimers of Li(Na)-based organometallic material provide relevant information about the vibrational properties of many possible solid reaction products. Such an approach should serve as a basis to extend existing spectral libraries of molecular structures relevant for understanding the link between atomic structures and measured spectroscopic data of materials in novel battery systems.

1. Introduction

Deployment of advanced next-generation battery systems has now become an attractive topic of research, involving multiple efforts that extend across academic and industrial laboratories.[1-5] Technologies that are actively developed include battery cells based on Li-ion materials, Li-sulfur, and Li-air. In every case the cell needs to have an electrolyte that conducts ions between the electrodes, and primarily organic electrolytes based on solvents such as ethylene carbonate or propylene carbonate are used. It is unavoidable that organic solvents come in contact and react with Li-containing materials, forming a variety of substances that significantly affect the performance and life of battery cells. Li-air batteries in particular received a lot of attention recently,[3, 6] due to the promise of very high energy density. The Li/O_2 battery system (or Li-air battery) uses a lithium metal negative electrode and a positive electrode that electrochemically reduces atmospheric oxygen; hence the cathode active material is not always stored in the battery. Recent studies demonstrated that the oxygen anion species of the Li-air battery tend to react very promptly with common carbonate-based electrolytes. As a result, a variety of by-products are formed instead of the desired reaction product which is lithium peroxide.[2, 7-9] The path towards understanding these parasitic reactions and designing more stable solvents starts with clarifying the reaction by-products. Similarly, in Li-ion intercalation batteries electrode passivation plays a key role in the initial stages of battery operation. Typically a spontaneous self-terminating reaction between an electrode and the electrolyte forms an electrically insulating film called the solid-electrolyte interphase (SEI), whose function is to encapsulate and protect the electrode materials. This process is still poorly understood, and is actively researched, with the goal of better controlling the composition and morphology of the SEI through inclusion of various additives and surfactants. Very recently the class of Na-ion batteries has attracted interest in the energy storage field as a potentially lower-cost and more durable alternative to Li-ion batteries.[10] As the research efforts are just beginning, there is even less understanding than in the Li-ion case of the SEI formation and electrode-electrolyte reactions taking place in these advanced battery systems.

Common tools used to help with understanding of film-forming processes are spectroscopic techniques such as Raman, FTIR, NMR, XPS, etc. They have been used to investigate the electrochemical reaction pathways and the composition of the SEIs.[11-15] In such studies it is common to involve direct chemical synthesis followed by spectroscopy measurements of the possible reaction products (as derived from theoretically proposed reaction mechanisms) to decipher the contents of the SEI or discharge reaction products of Li-air batteries. This strategy, however, is

limited by the need of careful synthesis and purification of a plethora of possible species resulting from the interaction of electrodes and solvents. It is, therefore, crucial to develop a database of the spectroscopic signatures of relevant organo-metallic compounds that can be used to match the spectra measured from electrode samples. Thus there is a need to explore more efficient approaches that could expedite the characterization of the species and building up of such libraries of fingerprints.

In this study, we elaborate on the possibilities of using first-principles computations to expedite spectroscopic characterization of possible reaction by-products in the Li- and Na-based battery systems. Some efforts in this direction have already been pursued;[12, 16] those studies mainly focused on the simulation of the infrared (IR)-characteristics of the SEI layers of typical Li-ion batteries. However, we believe that Raman spectroscopy is a more diagnostic and convenient characterization tools for studying electrochemical products because it offers a better band separation and narrower bandwidths, avoiding complex spectral profiles as observed with infrared spectroscopy. Also, to the best of our knowledge only few reports have integrated the use of Raman spectroscopy simulations to identify species and chemical processes in the development of lithium-based battery systems.[17, 18] Therefore, the primary focus of the present study is to develop a systematic approach of using first-principles calculations to predict Raman spectra and to construct a library of signatures of possible electrochemical reaction products relevant to the Li-air and Li/Na-ion battery systems.

As shown below, Raman activities of the possible Li-air reaction products (i.e., lithium oxide (Li_2O) and Li_2O_2) computed with periodic linear response methods compare quite well with experimental data. Such an approach requires prior knowledge of the crystalline parameters. However, often the solid-state crystalline structure of relevant organometallic compounds for batteries is often unknown or even irrelevant (for amorphous solids). For example, the computation of Raman signatures for a series of compounds (i.e., lithium acetate (CH_3CO_2Li), lithium formate (HCO_2Li), lithium-methyl carbonate (CH_3OCO_2Li), lithium methoxide (CH_3OLi), and lithium oxalate ($Li_2C_2O_4$)) that have been proposed as possible discharge reaction by-products of a Li-air battery[2, 7-9, 19] is challenging due to the lack of sufficient crystallographic information.. On the basis of a systematic investigation, we demonstrate that molecular dimers of Li/Na-based organometallic material provide relevant information about the vibrational properties of many possible solid reaction products, by comparing with experimental spectra. Additionally, since the crystallographic structure for Li/Na oxalates and HCO_2Na has been already reported,[20-22] we were able to compare the Raman characteristics derived from the dimer-approach to those Raman activities estimated using the periodic linear response formalism, also achieving a good agreement with the experimental Raman data of these compounds. In those instances for which no-prior spectra were available (i.e., CH_3OCO_2Na, CH_3OLi, and CH_3ONa) we used a computational approach to estimate for the first time their respective vibrational and Raman signatures.

2. Methodology

2.1 Raman Spectroscopy

Raman spectroscopy is a widely used tool for the characterization of materials. This vibrational technique probes the potential energy surface of the atoms in the neighbourhood of the equilibrium lattice geometry, and therefore, it provides information in terms of the structural properties and chemical bonds. Raman intensity peaks are related to the change in the polarizability of the system due to the deformation introduced by lattice vibrations. Therefore, when the polarizability changes with particular lattice vibrations, these vibrational modes are Raman active. The Raman tensors α^n are defined as:

$$\alpha_{ij}^{n} = \sqrt{V}\sum_{Ik}\frac{\partial \chi_{ij}}{\partial r_{Ik}}u_{Ik}^{n} \qquad (1)$$

where χ_{ij} is the dielectric polarizability tensor, V is volume, and u_{Ik}^{n} is the atomic displacement associated with the vibrational mode *n*. The third rank tensors $\partial\chi_{ij}/\partial r_{Ik}$ can also be expressed as the second derivatives of the forces (F_{Ik}) with respect to the electric field ($\vec{E}$):

$$\frac{\partial \chi_{ij}}{\partial r_{Ik}} = \frac{1}{V}\frac{\partial^3 E_{tot}}{\partial r_{Ik}\partial \vec{E}_i \partial \vec{E}_j} = -\frac{1}{V}\frac{\partial^2 F_{Ik}}{\partial \vec{E}_i \partial \vec{E}_j} \qquad (2)$$

The Raman tensors as defined above can be computed either from the linear-response theory formalism or from finite differences:either as the derivative of the energy with respect to electric fields and atomic displacements,[23, 24] or as the derivative of the polarizability tensor χ_{ij} with respect to atomic displacements.[25, 26]

2.2 Computational Details

Accurate computation of Raman intensities is more difficult than the computation of the IR intensities because Raman intensities depend on polarizability derivatives, which require accurate sampling of the electron density via large and diffuse basis sets.[27] Previous studies [28, 29] found that hybrid functionals (e.g., B3LYP and B3PW91), in combination with the medium-sized Sadlej polarized-valence double zeta basis set are suitable for accurate prediction of Raman intensities. The PBE0 functional in combination with the TZVPPD basis set has also been used for obtaining accurate Raman characteristics of medium-size organic molecules.[30] We have estimated the vibrational frequencies and their respective Raman activities and band assignments for the molecular dimers shown in Figure 1 using both combinations. No significant differences were found between the two, and we chose the less computationally expensive B3PW91/Sadlej combination for the computations presented below. First-principles calculations of dimer molecular structures were performed using the GAMESS code.[31] Vibrational frequency analysis was performed to ensure that optimized structures were minima (zero imaginary frequencies). Calculated vibrational frequencies tend to exceed the experimental values; therefore the vibrational frequencies reported in this study have been scaled by the empirical factor of 0.9674 as determined by Halls et al.[28] for the B3PW91/Sadlej model chemistry. In the case of the PBE0 hybrid functional[32] and the TZVPPD basis set[33], the vibrational

frequencies were scaled by the empirical factor of 0.9594, which is the reported scale factor for the DFT/PBE0/6-311+G(d,p) combination.[34] The calculated Raman activities reported for the molecular dimers reported in this study were estimated by a numerical differentiation procedure as implemented in the GAMESS code.

It is important to note that in this work, we calculated only the Raman activities as a way to obtain a qualitative estimate of the relative intensities of the Raman peaks for the crystalline and molecular compounds. In principle, our calculated Raman activities could be used to obtain theoretical Raman intensities as described in Reference [35]; however, the calculation of the theoretical Raman intensities also requires experimental information not readily available for all the experimental Raman spectra used in this study. To facilitate comparison with the experimental spectra, the calculated Raman activities have been normalized with respect to the strongest peaks found in specific frequency regions of the corresponding Raman spectrum.

For periodic crystalline structure, the electronic minimization and optimization of the atomic positions and unit cell parameters were computed using the local density approximation (LDA) of DFT as implemented in the Quantum Espresso package.[36]. Troullier-Martins norm-conserving LDA pseudopotentials were used for Li, O, C, and H.[37] Phonon frequencies were obtained from the linear-response calculation of the dynamical matrix in the harmonic approximation Raman tensors were obtained using density functional perturbation theory[38] as implemented in the Raman module of Quantum Espresso.[24] We used a 150 Ry cut-off energy for the kinetic energy. Brillouin-zone integration was performed with *k*-points in a Monkhorst-Pack scheme:[39] (6,6,6), (6,6,6), (6,4,2), (6,4,2), (4,4,4) for the primitive unit cell of Li_2O, Li_2O_2, $Li_2C_2O_4$, $Na_2C_2O_4$, and HCO_2Na, respectively.

The calculated Raman spectra are plotted with Gaussian functions with a full width at half-height of 10 cm^{-1}.

2.3 Dimer approach to Raman Spectra of Organometallic Compounds

To provide an accurate description of the vibrational properties of the discharge reaction products, a relevant molecular-level model system that effectively accounts for the intra- and intermolecular interactions is required. We propose to represent solid-state Li/Na organometallic compounds with dimers, for the purposes of Raman spectra predictions. The intuition leading to this approach suggests that upon crystallization of these molecular units, the intramolecular vibrations (especially the high-frequency ones) are insensitive to the ordering. Therefore, even if the details of the crystal structure are not known, or if molecules do not crystallize in an ordered fashion, information can still be obtained using the dimer representation. Previous reports have indicated that calculated vibrational spectra of dimer molecular representations are significantly more accurate than those of monomers.[40-43] For example, Zhuang et al.,[44] Matsusa et al.,[45] and Dedryvère et al.[12] have used dimer model calculations to assist in the interpretation of the IR and XPS spectra of various Li-based organometallic compounds appearing in Li-ion batteries. In these studies the explicit inclusion of O-Li-O intermolecular interactions, where Li ions are shared by two unit molecules, was key to allow exploration of the effect of the intermolecular interactions on the spectroscopic signatures of the investigated Li-based organometallic systems. In this study, we adopt a similar approach and apply it to case of Raman spectroscopy for the first time.

3. Results and Discussion

3.1 Structural Information of the Investigated Molecular Materials

Table 1 collects the experimental and DFT/LDA optimized parameters of the five periodic crystals studied in this work. Li_2O crystallizes in a cubic antifluorite structure (α phase, space group *Fm*-3*m*).[46] Each Li ion is tetrahedrally coordinated to four O atoms, and each O atom occupies the center of a cube formed by eight Li atoms. Li_2O_2 crystallizes in a hexagonal structure ($P6_3/mmc$ space group).[47] Oxygen atoms form O_2 pairs; half of the Li ions are at the center of a triangular prism made by six O atoms; and the other half lie in an octahedral site formed as well by six Li atoms. $Li_2C_2O_4$,[20] $Na_2C_2O_4$,[21] and HCO_2Na[22] have all monoclinic structure with space group $P2_1/n$, $P2_1/c$, and $P2_1/c$ respectively.

For the rest of the compounds discussed in this study (i.e., CH_3CO_2Li, HCO_2Li, CH_3OCO_2Li, CH_3OLi, $Li_2C_2O_4$ and their corresponding Na-analogs) molecular dimers were used to approximately represent the crystalline packing of these compounds in the solid state. In Figure 1, we present the optimized molecular dimers of CH_3CO_2Li, HCO_2Li, CH_3OCO_2Li, CH_3OLi, and $C_2O_4Li_2$ (and their corresponding Na-analogs). The atomic coordinates of the molecular structures shown in Figure 1 are provided in Tables S1-S5. Also in Tables S6-S10 we present the DFT/PBE0/TZVPPD optimized coordinates of the same molecular structures.Tables S11-S15 contain the vibrational frequencies and band assigments for the various Li/Na molecular dimers as obtained with the DFT/PBE0/TZVPPD method.

Table 1. DFT/LDA optimized unit cell parameters for Li_2O, Li_2O_2, $Li_2C_2O_4$, $Na_2C_2O_4$, and HCO_2Na.

Li_2O		Li_2O_2		$Li_2C_2O_4$		$Na_2C_2O_4$		HCO_2Na	
a (Å)	4.489	*a* (Å)	3.059	*a* (Å)	3.166	*a* (Å)	3.543	*a* (Å)	6.462
		c (Å)	7.437	*b* (Å)	5.074	*b* (Å)	5.469	*b* (Å)	6.991
				c (Å)	8.907	*c* (Å)	10.563	*c* (Å)	6.186
				β (°)	97.536	*β* (°)	90.757	*β* (°)	117.933

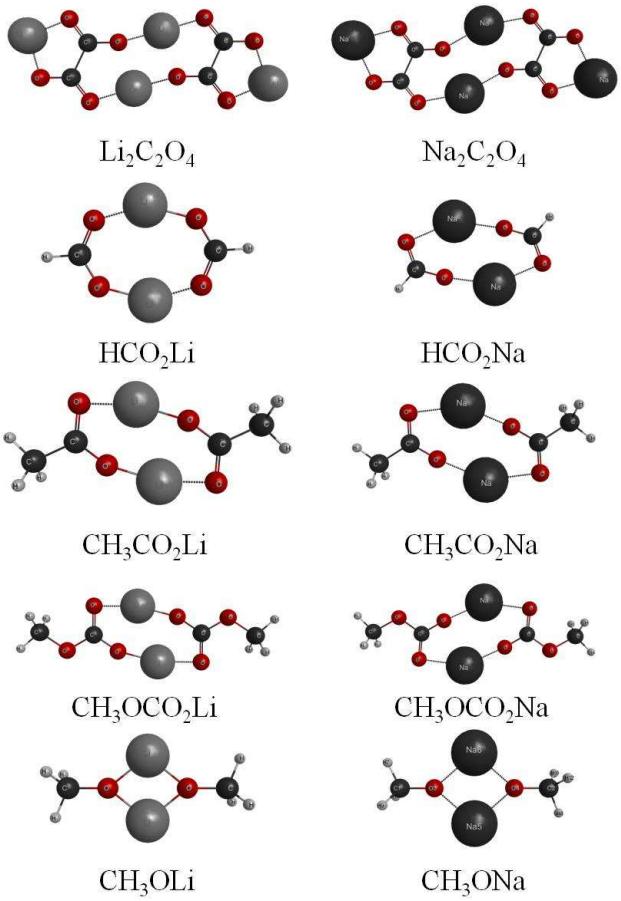

Figure 1. DFT/B3PW91/Sadlej optimized structures of the various molecular dimers investigated in this study. The optimized atomic coordinates are provided in Tables S1-S5.

3.2 Experimental and Theoretical Raman Spectra of the Main Reaction Products of the Li-air Battery: Li_2O and Li_2O_2

The calculated and experimentally measured Raman spectra for the possible Li-air electrochemical reaction products are shown in Figure 2. Li_2O and Li_2O_2 each show one very intense Raman-active vibrational mode at around 523 cm^{-1} [48] and 790cm^{-1} [49], respectively. A good agreement is found between the experimental and the first-principles computed frequencies of these vibrational modes; for example, our calculations show these normal modes to have frequencies of 566 cm^{-1} and 834 cm^{-1} for Li_2O and Li_2O_2, respectively. Given such spectroscopic features, one should expect to clearly distinguish the presence of the crystalline form of Li_2O versus that of Li_2O_2. An analysis of the eigenvector displacements of the respective normal-mode vibrations of Li_2O and Li_2O_2 shows that the 566 cm^{-1} vibrational mode in Li_2O is characterized by centro-symmetric displacements of the lithium atoms against each other, while the oxygen atoms remain motionless. The 834 cm^{-1} vibrational mode in Li_2O_2 corresponds to lateral centro-symmetric displacements of the oxygen atoms. If one then takes into account the results presented in the next section for the various Li-air reactions by-products, we note that if the desired Li-air reaction product Li_2O_2 electrochemically forms, its characteristic Raman signature should be clearly distinguishable from those other reaction by-products.

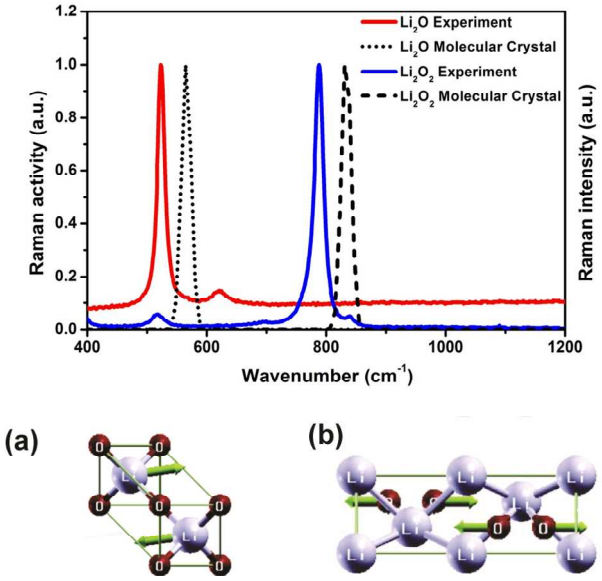

Figure 2. Experimental and theoretical Raman signatures for Li_2O and Li_2O_2. The eigenvectors of the most intense Raman active vibrations for a) Li_2O and b) Li_2O_2 are also shown. The experimental data are courtesy of IBM Almaden Research Center.

3.3 Experimental and Theoretical Raman Spectra of Organometallic Compounds

Figures 3-7 present DFT-simulated Raman activities of the compounds reported in Figure 1. For better comparison with the available experimental data, the simulated Raman peaks in Figures 3-7 have been normalized with respect to the strongest peaks found in the 400-2000 cm^{-1} and 2800-3200 cm^{-1} regions. We note that for the majority of the compounds reported in this study, their respective band assignments have been already discussed in previous studies on the basis of experimental studies,[11, 50-55]; therefore, we present the assignment of the bands resulting from the use of the DFT/B3PW91/Sadlej computational methodology for the dimer structures shown in Figure 1. The nomenclature used in this study for the band assignments corresponds to υ, δ, and τ for stretching, bending, and torsion vibrations respectively.

3.3.1 Lithium and Sodium Oxalate

Figure 3 shows the comparison of the experimental and DFT results for the Raman spectra of $Li_2C_2O_4$ and $Na_2C_2O_4$. Table 2 summarizes the vibrational frequencies and their corresponding band assignments. As shown in Figure 3, there is a good agreement between the calculated vibrational frequencies and Raman activities obtained from the molecular-dimer approach and the crystalline-structure-based method and the experimental results collected by Edwards and Lewis.[52] The spectroscopic

analysis reveals the presence of 3 prominent peaks, which are similar in vibronic nature between $Li_2C_2O_4$ and $Na_2C_2O_4$. According to the theoretical band assignments, the low-frequency bands (400-700 cm^{-1}) of these compounds are quite different; for example, the $Li_2C_2O_4$ compound has twice as many low-frequency vibrations as the $Na_2C_2O_4$ compound. As intuited, in many of these low-frequency vibrations, the light-weight Li-atom is involved. We note also an excellent agreement between the normalized values of the Raman activities as obtained from the crystalline structure of both oxalates and from their respective low-energy molecular dimers. This agreement further highlights the practicality of using molecular-dimer computations, as a quick approach to estimate the Raman signatures of organometallic systems that could form as a result of electrolyte-decomposition reactions in advanced lithium/sodium-based battery systems.

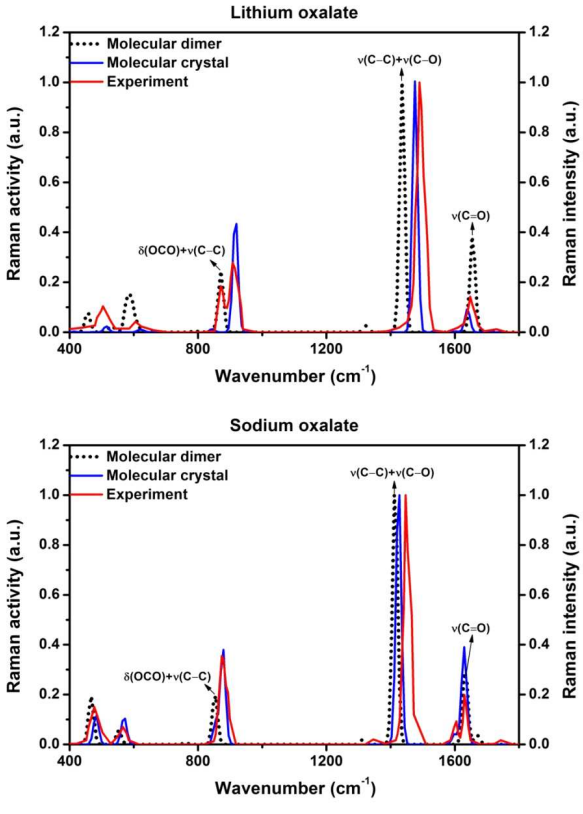

Figure 3. Experimental[52] and calculated Raman signatures for $Li_2C_2O_4$ and $Na_2C_2O_4$. The labels of the peaks correspond to the band assignment obtained from the dimer-approach calculations.

Table 2. Calculated vibrational frequencies for dimers of $Li_2C_2O_4Li_2$ and $Na_2C_2O_4$ and their respective band assignments. The reported vibrational frequencies were scaled by 0.9674 (see text for details).

$Li_2C_2O_4$				$Na_2C_2O_4$		
(cm^{-1})	(Å^4/amu)	Assignment		(cm^{-1})	(Å^4/amu)	Assignment
1703	0	ν(C=O)		1671	3	ν(C=O)
1688	0	ν(C=O)		1663	0	ν(C=O)
1655	26	ν(C=O)		1632	23	ν(C=O)
1644	0	ν(C=O)		1619	0	ν(C=O)
1436	66	ν(C-C) + ν(C-O)		1414	79	ν(C-C) + ν(C-O)
1435	2	ν(C-C) + ν(C-O)		1413	0	ν(C-C) + ν(C-O)
1323	1	ν(OCO)		1314	2	ν(OCO)
1321	0	ν(OCO)		1313	0	ν(OCO)
878	0	δ(OCO) + ν(C-C)		853	14	δ(OCO) + ν(C-C)
871	16	δ(OCO) + ν(C-C)		853	1	δ(OCO) + ν(C-C)
852	0	δ(OCO) out of plane		846	1	δ(OCO) out of plane
852	0	δ(OCO) out of plane		845	0	δ(OCO) out of plane
806	0	δ(OCO)		761	0	δ(OCO)
788	0	δ(OCO)		760	0	δ(OCO)
663	0	ν(O-Li)		553	3	δ(OCC)
611	2	ν(O-Li)		552	1	δ(OCC)
594	8	δ(OCO) + ν(O-Li)		495	0	δ(OCO) out of plane
581	3	δ(OCO) + δ(O-Li)		495	0	δ(OCO) out of plane
577	5	δ(OCO) + δ(O-Li)		467	13	ν(C-C)
571	0	δ(OCO) + ν(O-Li)		465	2	ν(C-C)
534	0	δ(OCC) + δ(O-Li)				
531	2	δ(OCC) + δ(O-Li)				
500	0	δ(OCO) out of plane				
491	0	δ(OCO) out of plane				
464	0	ν(C-C)				
456	5	ν(C-C)				

3.3.2 Lithium and Sodium Formate

Figure 4 shows the comparison of the experimental and DFT results for the Raman spectra of HCO_2Li and HCO_2Na. In Table 3, we summarize the characteristic vibration frequencies and their corresponding band assignments of these two compounds. The data collected in Table 3 reveals that both formate compounds have the same band assignments for the simulated Raman activities obtained based in their respective molecular dimers. Our spectroscopy analysis for HCO_2Li (as derived from the dimer-approach simulations) reveals that the position of the peak corresponding to the in-plane bending motion of the C-H bond in the 1300-1400 cm^{-1} region with respect to highest intensity peak in the same spectroscopic region differs somewhat from the experimental spectra reported by Müller et al.[55] Experimentally, the OCO stretching vibration in HCO_2Li appears in the 1370-

1380 cm^{-1} range and the HCO bending vibration in the 1390-1400 cm^{-1} region. This shift between the stretching and bending vibrations also prevails when comparing the calculated vibrations and band assignments to the results reported by Heyns, A. M. for the crystalline phase of HCO_2Na[54]. For the case of the HCO_2Na compound, the OCO stretching and HCO bending vibrations as derived from the dimer approach appear at 1364 cm^{-1} and 1323 cm^{-1}, respectively (experimentally the ν (OCO) and the δ (HCO) appear at 1355 cm^{-1} and 1366 cm^{-1}, respectively). In order to investigate the origin of the discrepancy we performed computations of Raman activities of the periodic crystal structure of Na formate. Interestingly, the simulated Raman activities resulting from the DFT/LDA approach also coincide with the dimer-approach simulations (i.e., ν (OCO) and δ (HCO) at 1353 cm^{-1} and 1319 cm^{-1}, respectively (see Table S16), thus ruling out the possibilities of errors coming from computational approximations such as dimer structural representation or basis sets and functionals used. Despite the variations in these two vibrational frequencies, the experimental Raman intensities are again in good agreement with the normalized Raman activities obtained from the DFT methods (DFT/B3PW91/Sandlej and DFT/LDA, for the molecular dimer of HCO_2Na and for its crystalline structure, respectively).

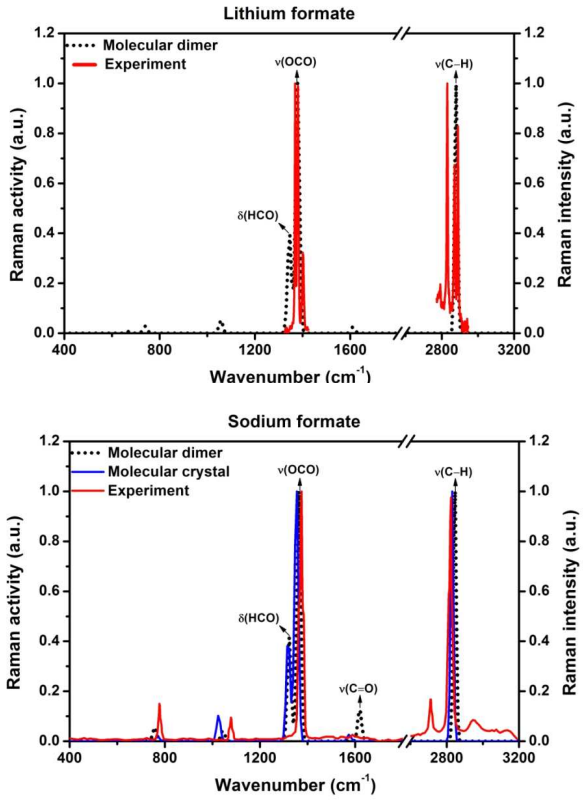

Figure 4. Experimental (from references [55] and [56] for HCO_2Li and HCO_2Na, respectively) and calculated Raman signatures for formates. Note: the feature at around 1400 cm^{-1} for the experimental spectrum of HCO_2Na consists of two peaks. Due to the digitalization of HCO_2Na Raman spectrum only one peak is shown here; see reference [56] for more details. The labels of the peaks correspond to the band assignment obtained from the dimer-approach calculations.

Table 3. Calculated vibrational frequencies for dimers of HCO_2Li and HCO_2Na and their respective band assignments. The reported vibrational frequencies were scaled by 0.9674 (see text for details).

HCO_2Li				HCO_2Na		
(cm^{-1})	(Å^4/amu)	Assignment		(cm^{-1})	(Å^4/amu)	Assignment
2879	334	ν(CH)		2845	402	ν(CH)
2877	0	ν(CH)		2843	3	ν(CH)
1652	0	ν(C=O)		1619	0	ν(C=O)
1612	1	ν(C=O)		1619	4	ν(C=O)
1379	27	ν(OCO)		1364	29	ν(OCO)
1378	0	ν(OCO)		1360	0	ν(OCO)
1345	11	δ(HCO)		1323	11	δ(HCO)
1345	0	δ(HCO)		1323	0	δ(HCO)
1057	1	τ(CH)		1045	0	τ(CH)
1056	0	τ(CH)		1044	1	τ(CH)
739	0	δ(OCO) + ν(O-Li)		759	0	δ(OCO)
739	1	δ(OCO)		758	2	δ(OCO)
688	0	ν(O-Li)				
670	0	ν(O-Li)				

3.3.3 Lithium and Sodium Acetate

Figure 5 shows the comparison of the experimental and computed results for the Raman spectra of CH_3CO_2Li and CH_3CO_2Na. In Table 4, we summarize the characteristic vibration frequencies and their corresponding band assignments. As shown in Figure 5 and despite the limited amount of Raman spectroscopy information for the specific case of CH_3CO_2Li, there is substantial agreement between the dimer-approach DFT-simulation of the Raman activities and the Raman experimental signatures of these two compounds. For these two compounds, a DFT simulation using the crystalline structure of these compounds (i.e., DFT/LDA approach) was not attempted because the structural information for CH_3CO_2Li is incomplete.[57] Raman signatures and band assignments have been discussed in the past for CH_3CO_2Na[53, 58] and CH_3CO_2Li[51]. According to our DFT analysis derived from a dimer structure for CH_3CO_2Li, between 7 and 9 salient Raman peaks are present in the Raman spectrum of CH_3CO_2Li. As observed in Table 4, almost the same vibrational band assignments, in terms of normal mode characteristics and vibrational frequencies were obtained from the DFT/B3PW91/Sadlej simulation of the dimer structure of CH_3CO_2Na. Although the normal mode analysis for the vibrational frequencies of CH_3CO_2Li reveals the presence of two O-Li stretching vibrations at approximately 690 cm^{-1}, the Raman activities for these two vibrational frequencies are negligible. Again, we were able to provide detailed information for the vibrational characteristics of molecular solids, which have not been fully characterized experimentally.

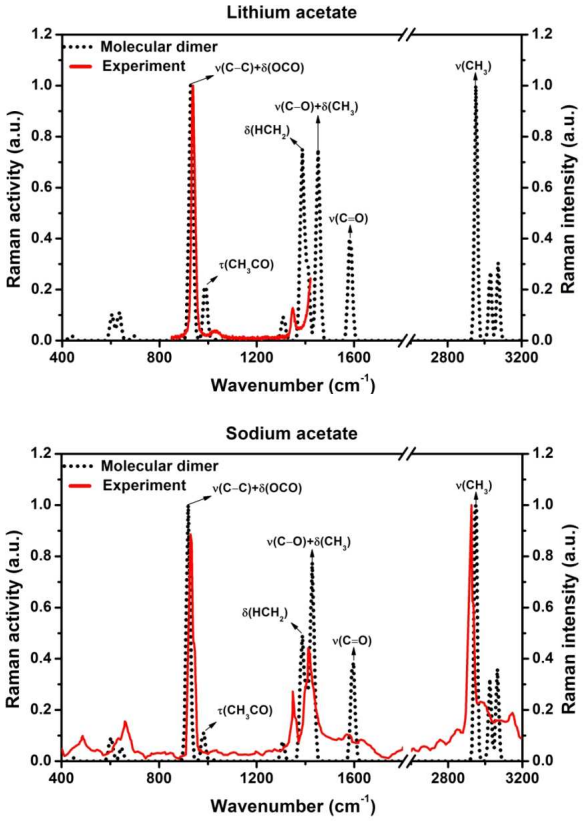

Figure 5. Experimental (from references [59] and [56] for CH_3CO_2Li and CH_3CO_2Na, respectively) and calculated Raman signatures for acetates. The labels of the peaks correspond to the band assignment obtained from the dimer-approach calculations.

Table 4. Calculated vibrational frequencies for dimers of CH_3CO_2Li and CH_3CO_2Na and their respective band assignments. The reported vibrational frequencies were scaled by 0.9674 (see text for details).

CH_3CO_2Li				CH_3CO_2Na		
3074	51	$\nu(HCH_2)$		3065	59	$\nu(HCH_2)$
3073	56	$\nu(HCH_2)$		3065	54	$\nu(HCH_2)$
3030	50	$\nu(HCH_2)$		3025	82	$\nu(HCH_2)$
3030	49	$\nu(HCH_2)$		3025	19	$\nu(HCH_2)$
2954	290	$\nu(CH)_3$		2948	296	$\nu(CH)_3$
2953	67	$\nu(CH)_3$		2948	57	$\nu(CH)_3$
1595	0	ν(C=O)		1596	0	ν(C=O)
1584	9	ν(C=O)		1594	12	ν(C=O)
1452	15	ν(C-O) + $\delta(CH_3)$		1428	22	ν(C-O) + $\delta(CH_3)$
1440	0	ν(C-O) + $\delta(CH_3)$		1420	0	ν(C-O) + $\delta(CH_3)$
1409	6	$\delta(HCH_2)$		1406	7	$\delta(HCH_2)$
1409	0	$\delta(HCH_2)$		1405	0	$\delta(HCH_2)$
1387	0	$\delta(HCH_2)$		1386	0	$\delta(HCH_2)$
1387	15	$\delta(HCH_2)$		1385	14	$\delta(HCH_2)$
1310	2	$\delta(CH_3)$ + ν(C-O)		1306	2	$\delta(CH_3)$ + ν(C-O)
1308	0	$\delta(CH_3)$ + ν(C-O)		1306	0	$\delta(CH_3)$ + ν(C-O)
1021	0	$\tau(CH_3CO)$		1014	0	$\tau(CH_3CO)$
1020	0	$\tau(CH_3CO)$		1014	0	$\tau(CH_3CO)$
992	0	$\tau(CH_3CO)$		982	1	$\tau(CH_3CO)$
988	5	$\tau(CH_3CO)$		981	3	$\tau(CH_3CO)$
942	0	ν(C-C) + δ(OCO)		922	0	ν(C-C) + δ(OCO)
930	21	ν(C-C) + δ(OCO)		920	28	ν(C-C) + δ(OCO)
692	0	ν(O-Li)		646	1	δ(OCO) + ν(C-C)
691	0	ν(O-Li)		645	0	δ(OCO) + ν(C-C)
642	0	δ(OCO) + ν(C-C)		603	0	δ(CCO) out of plane
634	2	δ(OCO) + ν(C-C)		602	3	δ(CCO) out of plane
607	0	δ(CCO) out of plane		451	0	δ(CCO) in plane
604	2	δ(CCO) out of plane		444	0	δ(CCO) in plane
450	0	δ(CCO) in plane				
436	0	δ(CCO) in plane				

5

3.3.4 *Lithium and Sodium Methyl Carbonate*

Figure 6 shows the comparison of the experimental and DFT results for the Raman spectra of CH_3OCO_2Li and CH_3OCO_2Na. Their respective vibration frequencies and their corresponding band assignments are reported in Table 5. Only recently, the experimental Raman spectrum of CH_3OCO_2Li has been reported;[7] but its respective vibrational band assignments based on IR spectroscopy studies have been extensively discussed in the past.[13, 14, 45] In Figure 6, we observe that overall, there is a good agreement between the calculated vibrational frequencies and Raman activities derived from the DFT-based dimer approach and the recent experimental Raman spectrum reported by McCloskey et al.[7] To the best of our knowledge, no Raman or IR has been previously presented for the CH_3OCO_2Na compound; thus, in the following, we will focus mainly on the description of the spectroscopic properties of CH_3OCO_2Na, which are very similar to those of CH_3OCO_2Li.

According to our DFT analysis derived from a dimer structure for CH_3OCO_2Na, approximately 9 salient Raman peaks should be present in the Raman spectrum of CH_3OCO_2Na; which are also similar to those present for the CH_3OCO_2Li compound as reported in Table 5. Almost all vibrations can be equally assigned to the both compounds, except for the presence of few O-Li stretching vibrations in CH_3OCO_2Li at approximately 690 cm^{-1}. The Raman activities for these modes are negligible compared to the largest activity in 400-2000 cm^{-1} region.

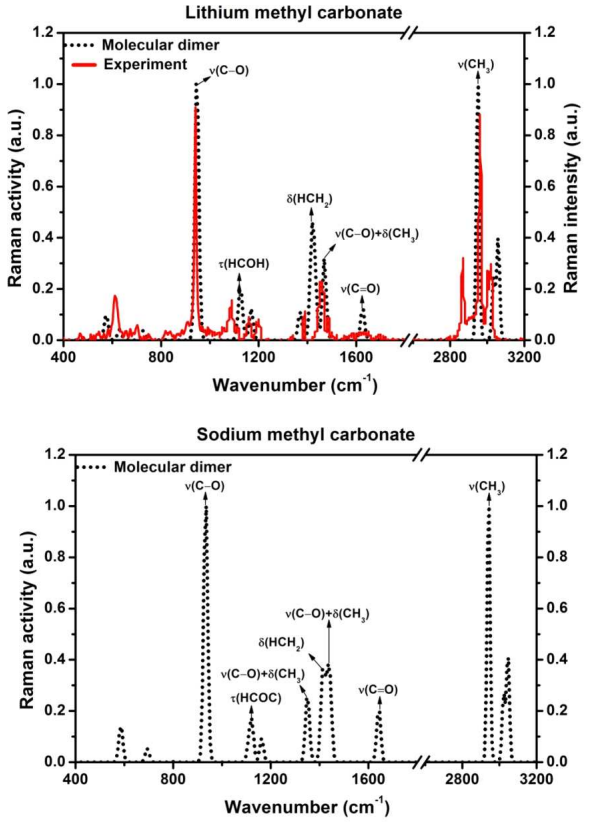

Figure 6. Experimental (only data for CH_3OCO_2Li; spectrum taken from Reference[7]) and calculated Raman signatures for CH_3OCO_2Li and CH_3OCO_2Na. The labels of the peaks correspond to the band assignment obtained from the dimer-approach calculations.

Table 5. Calculated vibrational frequencies for dimers of CH_3OCO_2Li and CH_3OCO_2Na and their respective band assignments. The reported vibrational frequencies were scaled by 0.9674 (see text for details).

CH_3OCO_2Li				CH_3OCO_2Na		
(cm^{-1})	(Å^4/amu)	Assignment		(cm^{-1})	(Å^4/amu)	Assignment
3059	32	$\nu(HCH_2)$		3046	0	$\nu(HCH_2)$
3059	106	$\nu(HCH_2)$		3046	150	$\nu(HCH_2)$
3034	32	$\nu(HCH_2)$		3022	20	$\nu(HCH_2)$
3034	52	$\nu(HCH_2)$		3022	72	$\nu(HCH_2)$
2950	36	$\nu(CH)_3$		2941	350	$\nu(CH)_3$
2950	323	$\nu(CH)_3$		2941	11	$\nu(CH)_3$
1632	0	ν(C=O)		1642	6	ν(C=O)
1625	4	ν(C=O)		1641	0	ν(C=O)
1469	9	ν(C-O) + $\delta(CH_3)$		1442	9	ν(C-O) + $\delta(CH_3)$
1456	0	ν(C-O) + $\delta(CH_3)$		1439	0	ν(C-O) + $\delta(CH_3)$
1430	7	$\delta(HCH_2)$		1429	6	$\delta(HCH_2)$
1429	0	$\delta(HCH_2)$		1427	0	$\delta(HCH_2)$
1418	8	$\delta(HCH_2)$		1413	4	$\delta(HCH_2)$
1417	2	$\delta(HCH_2)$		1412	7	$\delta(HCH_2)$
1370	3	ν(C-O) + $\delta(CH_3)$		1350	8	ν(C-O) + $\delta(CH_3)$
1360	0	ν(C-O) + $\delta(CH_3)$		1339	0	ν(C-O) + $\delta(CH_3)$
1171	0	τ(HCOC)		1163	2	τ(HCOC)
1169	3	τ(HCOC)		1161	0	τ(HCOC)
1126	6	τ(HCOC)		1122	0	τ(HCOC)
1126	0	τ(HCOC)		1122	4	τ(HCOC)
1117	0	ν(C-O)		1110	2	ν(C-O)
1116	1	ν(C-O)		1109	0	ν(C-O)
956	0	ν(C-O)		934	1	ν(C-O)
947	31	ν(C-O)		933	31	ν(C-O)
807	0	$\delta(CO_3)$ out of plane		806	0	$\delta(CO_3)$ out of plane
806	0	$\delta(CO_3)$ out of plane		805	0	$\delta(CO_3)$ out of plane
729	1	δ(O-C=O) + ν(O-Li)		694	0	δ(O-C=O)
718	0	δ(O-C=O) + ν(O-Li)		694	1	δ(O-C=O)
674	0	δ(COO) + ν(O-Li)		586	4	δ(O-C-O)
630	1	δ(COO) + ν(O-Li)		583	0	δ(O-C-O)
576	3	δ(O-C-O)				
559	0	δ(O-C-O)				

3.3.5 Lithium and Sodium Methoxide

In Figure 7, we report the simulated Raman activities obtained from the DFT/B3PW91/Sandlej method for the molecular dimers of CH_3OLi and CH_3ONa. To the best of our knowledge, there is no experimental Raman data for the anhydrous solid phases of these two materials. Likewise, no information is available on the possible crystal structures. Despite this lack of Raman spectroscopic data, the details of IR vibrational characteristics for the CH_3OLi compound have been already discussed.[11, 45] The data shown in Figure 7 and collected in Table 6 show close similarities between the spectroscopic properties of these two compounds, except for one frequency vibration below 600 cm^{-1}, which corresponds to the LiOLi bending vibration. In contrast to all other Li-based organometallic compounds investigated in this study, only the CH_3OLi compound has a Li vibration with a significant Raman activity in the low-frequency region of the spectrum.

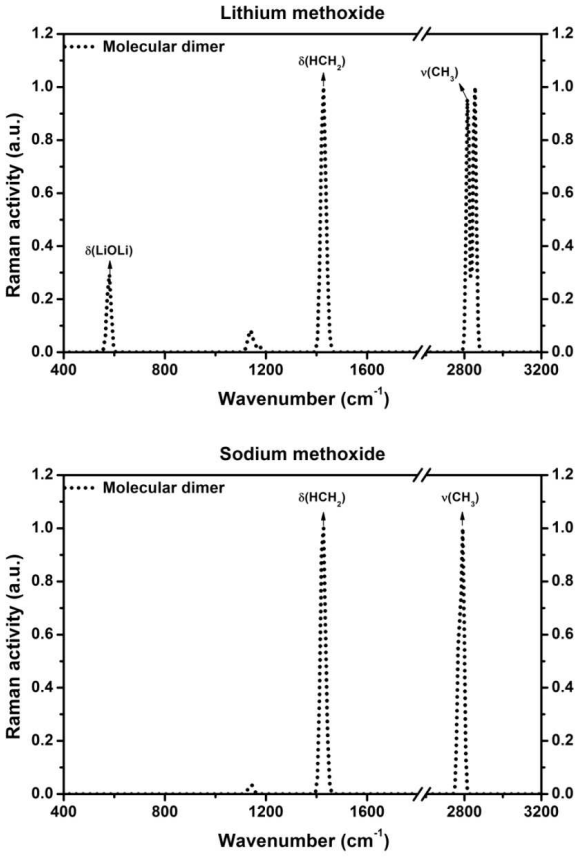

Figure 7. Calculated Raman signatures for CH_3OLi and CH_3ONa. The labels of the peaks correspond to the band assignment obtained from the dimer-approach calculations.

Table 6. Calculated vibrational frequencies for dimers of CH_3OLi and CH_3ONa and their respective band assignments. The reported vibrational frequencies were scaled by 0.9674 (see text for details).

CH_3OLi				CH_3ONa		
2856	3	$\nu(HCH_2)$		2792	1	$\nu(HCH_2)$
2856	235	$\nu(HCH_2)$		2792	375	$\nu(HCH_2)$
2851	5	$\nu(HCH_2)$		2791	26	$\nu(HCH_2)$
2851	267	$\nu(HCH_2)$		2791	345	$\nu(HCH_2)$
2818	470	$\nu(CH)_3$		2771	462	$\nu(CH)_3$
2813	0	$\nu(CH)_3$		2766	0	$\nu(CH)_3$
1438	9	$\delta(HCH_2)$		1436	9	$\delta(HCH_2)$
1435	0	$\delta(HCH_2)$		1434	0	$\delta(HCH_2)$
1428	17	$\delta(HCH_2)$		1426	13	$\delta(HCH_2)$
1427	0	$\delta(HCH_2)$		1426	6	$\delta(HCH_2)$
1421	17	$\delta(HCH_2)$		1420	18	$\delta(HCH_2)$
1420	0	$\delta(HCH_2)$		1420	0	$\delta(HCH_2)$
1170	1	ν(C-O)		1145	1	ν(C-O)
1151	0	ν(C-O)		1140	0	$\tau(OCH_3)$
1143	2	$\tau(OCH_3)$		1140	1	$\tau(OCH_3)$
1142	0	$\tau(OCH_3)$		1133	0	$\tau(OCH_3)$
1133	0	$\tau(OCH_3)$		1132	0	$\tau(OCH_3)$
1132	1	$\tau(OCH_3)$		1132	0	ν(C-O)
619	0	ν(O-Li)				
579	10	δ(LiOLi)				
546	0	ν(O-Li)				
516	0	δ(O-Li)				

3.3.6 Relevance of Larger Aggregates on the Raman Spectroscopic Signatures of CH_3OLi and CH_3ONa

To further test the dimer representation approach and explore the relevance of larger aggregates, we have also computed the Raman activities for two extended molecular aggregates. The selected configuration for the trimer and tetramer structures depicted in Figure 1, also maintain explicit O-Li(Na)-O intermolecular interactions, which are found to lead to stables structures.[43, 60] The computationally optimized coordinates of the molecular trimers and tetramers shown in Figure 8 are provided in Tables S17 and S18, respectively. For the case of CH_3OLi, the Raman peak position of the Li-Li stretching vibration located in low-frequency region of the respective Raman spectrum (400-600 cm^{-1}) shows some dependence on the aggregate size. Despite this observation and the presence of a larger number of peaks, our spectral simulations for larger aggregates confirm that there is indeed no substantial difference from the dimer predictions in terms of the peak positions and the nature of the band assignments. Thus, the proposed DFT-simulation of the Raman activities based on molecular dimers of organometallic complexes holds the promise of providing a tool to accurately predict the spectroscopic characteristics.

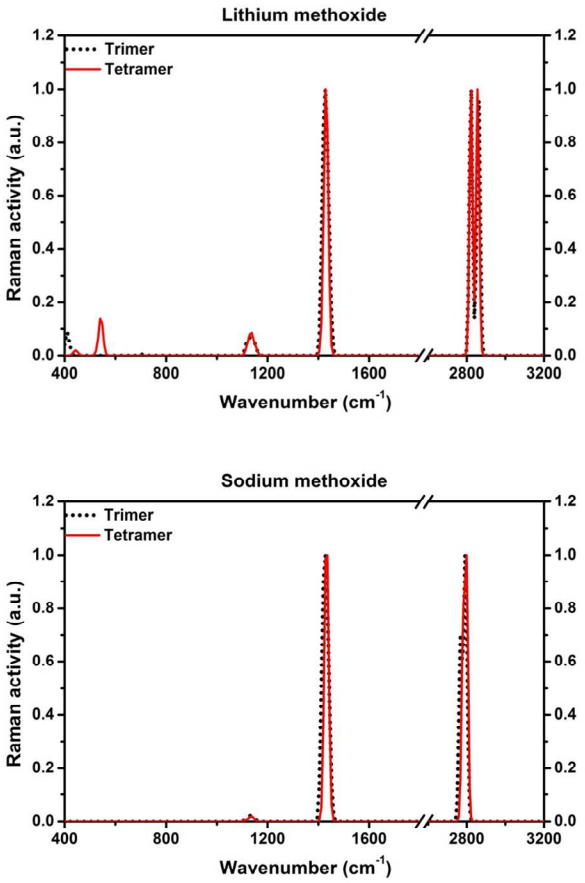

Figure 8. Calculated Raman signatures for larger aggregates of CH_3OLi and CH_3ONa.

4. Conclusions

We demonstrate that computational spectroscopy is a useful tool to assist experimental characterization of organometallic compounds present in Li batteries. We apply a novel dimer representation technique to compute Raman signatures of molecular solids which are difficult to isolate or for which crystalline structure is not known. On the basis of a systematic *ab-initio* investigation in this study, we demonstrate that small molecular dimers of Li/Na organometallic compounds can provide relevant information about the inter- and intramolecular interactions of their respective crystallographic configurations, which in turn leads to an improved description of their respective Raman spectra. As a result, we are able to construct a computed library of spectroscopic signatures of several classes of reaction products usually found in Li- and Na- based batteries, as well as Li-air batteries. Our theoretical characterization of Raman signatures of possible electrochemical reaction products indicates that combined computational and experimental Raman spectroscopy can be a very useful diagnostic tool to identify organic electrolyte reaction mechanisms and products in advanced batteries. We expect that approaches presented in this study can lead to establishing a database of spectroscopic fingerprints of a range of molecular structures relevant to developing deeper understanding of electrochemical process occurring at electrode-electrolyte interfaces of next-generation energy storage devices.

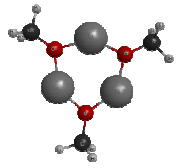

Trimer

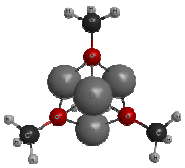

Tetramer

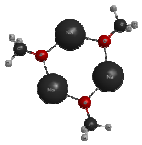

Trimer

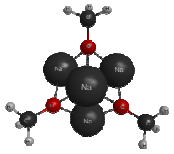

Tetramer

Acknowledgements

We thank Dr. J. Christensen, Dr. P. Albertus, and Dr. T. Lohmann for stimulating discussions.

Notes and references

Research and Technology Center North America, Robert Bosch LLC, Cambridge, Massachusetts 02140, USA. E-mail: boris.kozinsky@us.bosch.com

† Electronic Supplementary Information (ESI) available: DFT/B3PW91/Sadlej and DFT/PBE0/TZVPPD optimized atomic coordinates for molecular structures shown in Figure 1; DFT/PBE0/TZVPPD vibrational frequencies for dimers shown in Figure 1 and their respective band assignments; DFT/LDA vibrational frequencies for the crystalline structure of HCO_2Na and its respective band assignments; DFT/B3PW91/Sadlej optimized atomic coordinates for trimers and tetramers of CH_3OLi and CH_3ONa.

See DOI: 10.1039/b000000x/

1 P. Albertus, G. Girishkumar, B. McCloskey, R. S. Sanchez-Carrera, B. Kozinsky, J. Christensen and A. C. Luntz, *Journal of The Electrochemical Society*, 2011, **158**, A343-A351-A343-A351.

2 S. A. Freunberger, Y. Chen, Z. Peng, J. M. Griffin, L. J. Hardwick, F. Bardé, P. Novák and P. G. Bruce, *Journal of the American Chemical Society*, 2011, 8040–8047.

3 G. Girishkumar, B. McCloskey, A. C. Luntz, S. Swanson and W. Wilcke, *J. Phys. Chem. Lett.*, 2010, **1**, 2193-2203.

4 C. O. Laoire, S. Mukerjee, E. J. Plichta, M. A. Hendrickson and K. M. Abraham, *Journal of The Electrochemical Society*, 2011, **158**, A302-A308-A302-A308.

5 S. J. Visco, E. Nimon and L. C. De Jonghe, ed. G. Jürgen, Elsevier, Amsterdam, 2009, pp. 376-383.

6 J. Christensen, P. Albertus, R. S. Sanchez-Carrera, T. Lohmann, B. Kozinsky, R. Liedtke, J. Ahmed and A. Kojic, *Journal of The Electrochemical Society*, 2012, **159**, R1-R30.

7 B. D. McCloskey, D. S. Bethune, R. M. Shelby, G. Girishkumar and A. C. Luntz, *The Journal of Physical Chemistry Letters*, 2011, 1161-1166.

8 J. Xiao, J. Hu, D. Wang, D. Hu, W. Xu, G. L. Graff, Z. Nie, J. Liu and J.-G. Zhang, *Journal of Power Sources*, 2011, **196**, 5674-5678.

9 W. Xu, K. Xu, V. V. Viswanathan, S. A. Towne, J. S. Hardy, J. Xiao, Z. Nie, D. Hu, D. Wang and J.-G. Zhang, *Journal of Power Sources*, 2011, **196**, 9631-9639.

10 Technology Review Web: http://www.technologyreview.com/news/416488/sodium-ion-cells-for-cheap-energy-storage/ (accessed December 15, 2012).

11 D. Aurbach, M. L. Daroux, P. W. Faguy and E. Yeager, *Journal of The Electrochemical Society*, 1988, **135**, 1863-1871.

12 R. Dedryvère, L. Gireaud, S. Grugeon, S. Laruelle, J. M. Tarascon and D. Gonbeau, *The Journal of Physical Chemistry B*, 2005, **109**, 15868-15875.

13 L. Gireaud, S. Grugeon, S. Laruelle, S. Pilard and J.-M. Tarascon, *Journal of The Electrochemical Society*, 2005, **152**, A850-A857.

14 K. Xu, G. V. Zhuang, J. L. Allen, U. Lee, S. S. Zhang, P. N. Ross and T. R. Jow, *The Journal of Physical Chemistry B*, 2006, **110**, 7708-7719.

15 G. V. Zhuang, K. Xu, T. R. Jow and P. N. Ross, *Electrochemical and Solid-State Letters*, 2004, **7**, A224-A227.

16 X. Zhang, J. K. Pugh and Ross, Jr., *Electrochemical and Solid-State Letters*, 2001, **4**, A82-A84-A82-A84.

17 R. Aroca, M. Nazri, G. A. Nazri, A. J. Camargo and M. Trsic, *Journal of Solution Chemistry*, 2000, **29**, 1047-1060.

18 D. Battisti, G. A. Nazri, B. Klassen and R. Aroca, *The Journal of Physical Chemistry*, 1993, **97**, 5826-5830.

19 F. Mizuno, S. Nakanishi, Y. Kotani, S. Yokoishi and H. Iba, *Electrochemistry*, 2010, **78**, 403-405.

20 20 B. Beagley and R. W. H. Small, *Acta Crystallographica*, 1964, **17**, 783-788.

21 E. V. Boldyreva, H. Ahsbahs, V. V. Chernyshev, S. N. Ivashevskaya and A. R. Oganov, *Zeitschrift für Kristallographie - Crystalline Materials*, 2006, **221**, 186-197.

22 H. Fuess, J. W. Bats, H. Dannohl, H. Meyer and A. Schweig, *Acta Crystallographica Section B*, 1982, **38**, 736-743.

23 G. Deinzer and D. Strauch, *Physical Review B*, 2002, **66**.

24 M. Lazzeri and F. Mauri, *Physical Review Letters*, 2003, **90**, 036401.

25 B. G. Johnson and J. Florián, *Chemical Physics Letters*, 1995, **247**, 120-125.

26 P. Umari and A. Pasquarello, *Diamond and Related Materials*, 2005, **14**, 1255-1261.

27 M. D. Halls and H. B. Schlegel, *Comparison study of the prediction of Raman intensities using electronic structure methods*, AIP, 1999.

28 M. D. Halls, J. Velkovski and H. B. Schlegel, *Theor. Chem. Acc.*, 2001, **105**, 413-421.

29 E. E. Zvereva, A. R. Shagidullin and S. A. Katsyuba, *J. Phys. Chem. A*, 2011, **115**, 63-69.

30 D. Rappoport and F. Furche, *The Journal of Chemical Physics*, 2007, **126**, 201104.

31 M. W. Schmidt, K. K. Baldridge, J. A. Boatz, S. T. Elbert, M. S. Gordon, J. H. Jensen, S. Koseki, N. Matsunaga, K. A. Nguyen, S. Su, T. L. Windus, M. Dupuis and J. A. Montgomery, *Journal of Computational Chemistry*, 1993, **14**, 1347-1363.

32 C. Adamo and V. Barone, *The Journal of Chemical Physics*, 1999, **110**, 6158-6170.

33 D. Rappoport and F. Furche, *The Journal of Chemical Physics*, 2010, **133**, 134105.

34 J. P. Merrick, D. Moran and L. Radom, *The Journal of Physical Chemistry A*, 2007, **111**, 11683-11700.

35 E. C. Le Ru, P. G. Etchegoin and I. Books24x, *Principles of surface-enhanced Raman spectroscopy [electronic resource] : and related plasmonic effects / Eric C. Le Ru, Pablo G. Etchegoin*, Elsevier, Amsterdam :, 2009.

36 G. Paolo and et al., *Journal of Physics: Condensed Matter*, 2009, **21**, 395502.

37 N. Troullier, J. Martins, eacute and Luriaas, *Physical Review B*, 1991, **43**, 1993.

38 S. Baroni, S. de Gironcoli, A. Dal Corso and P. Giannozzi, *Rev. Mod. Phys.*, 2001, **73**, 515-562.

39 H. J. Monkhorst and J. D. Pack, *Physical Review B*, 1976, **13**, 5188.

40 J. Aaltonen, K. C. Gordon, C. J. Strachan and T. Rades, *International Journal of Pharmaceutics*, 2008, **364**, 159-169.

41 E. Koglin, D. Koglin, R. J. Meier and S. van Heel, *Chemical Physics Letters*, 1998, **290**, 99-104.

42 M. M. Nolasco, A. M. Amado and P. J. A. Ribeiro-Claro, *Journal of Raman Spectroscopy*, 2009, **40**, 394-400.

43 Y. Wang and P. B. Balbuena, *The Journal of Physical Chemistry A*, 2002, **106**, 9582-9594.

44 G. V. Zhuang, H. Yang, Ross, Jr., K. Xu and T. R. Jow, *Electrochemical and Solid-State Letters*, 2006, **9**, A64-A68-A64-A68.

45 S. Matsuta, T. Asada and K. Kitaura, *Journal of The Electrochemical Society*, 2000, **147**, 1695-1702.

46 T. W. D. Farley and et al., *Journal of Physics: Condensed Matter*, 1991, **3**, 4761.

47 H. Föppl, *Zeitschrift für anorganische und allgemeine Chemie*, 1957, **291**, 12-50.

48 J.-M. Hur, C.-S. Seo, S.-S. Hong, D.-S. Kang and S.-W. Park, *Reaction Kinetics and Catalysis Letters*, 2003, **80**, 217-222.

49 T. Ogasawara, A. Debart, M. Holzapfel, P. Novak and P. G. Bruce, *J. Am. Chem. Soc.*, 2006, **128**, 1390-1393.

50 W. Behrendt, G. Gattow and M. Dräger, *Zeitschrift für anorganische und allgemeine Chemie*, 1973, **397**, 237-246.

51 M. Cadene, *Journal of Molecular Structure*, 1968, **2**, 193-208.

52 H. G. M. Edwards and I. R. Lewis, *Spectrochimica Acta Part A: Molecular Spectroscopy*, 1994, **50**, 1891-1898.

53 R. L. Frost and J. T. Kloprogge, *Journal of Molecular Structure*, 2000, **526**, 131-141.

54 A. M. Heyns, *The Journal of Chemical Physics*, 1986, **84**, 3610-3616.

55 K. Müller, M. Heyns A, K. J. Range and M. Zabel, *Zeitschrift für Naturforschung. B.*, 1992, **47**, 238-246.

56 R. A. Nyquist, C. L. Putzig, M. A. Leugers and R. O. Kagel, *The handbook of infrared and Raman spectra of inorganic compounds and organic salts / Richard A. Nyquist, Curtis L. Putzig, and M. Anne Leugers*, Academic Press, San Diego :, 1997.

57 C. Saunderson and R. B. Ferguson, *Acta Crystallographica*, 1961, **14**, 321.

58 H. Noma, Y. Miwa, I. Yokoyama and K. Machida, *Journal of Molecular Structure*, 1991, **242**, 207-219.

59 RASMIN Web: http://riodb.ibase.aist.go.jp/rasmin/ (National Institute of Advanced Industrial Science and Technology, accessed October 2, 2012).

60 L. M. Pratt, O. Kwon, T. C. Ho and N. Van Nguyen, *Tetrahedron*, 2008, **64**, 5314-5321.

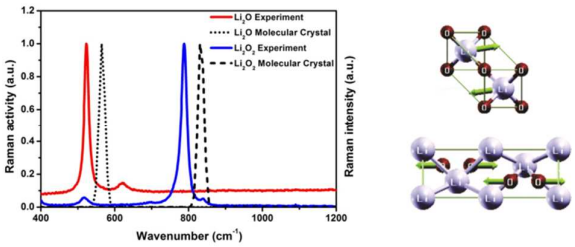

We demonstrate that small molecular dimers of Li/Na organometallic compounds can provide relevant information about the inter- and intramolecular interactions of their respective crystallographic configurations, which in turn leads to an improved description of their respective Raman spectra.